NASA Technical Memorandum 100430

Formulation of a General Technique for Predicting Pneumatic Attenuation Errors in Airborne Pressure Sensing Devices

Stephen A. Whitmore

May 1988

NASA
National Aeronautics and
Space Administration

NASA Technical Memorandum 100430

Formulation of a General Technique for Predicting Pneumatic Attenuation Errors in Airborne Pressure Sensing Devices

Stephen A. Whitmore
Ames Research Center, Dryden Flight Research Facility, Edwards, California

1988

National Aeronautics and
Space Administration
Ames Research Center
Dryden Flight Research Facility
Edwards, California 93523-5000

FORMULATION OF A GENERAL TECHNIQUE FOR PREDICTING PNEUMATIC ATTENUATION ERRORS IN AIRBORNE PRESSURE SENSING DEVICES

Stephen A. Whitmore*
NASA Ames Research Center
Dryden Flight Research Facility
Edwards, California

Abstract

Presented is a mathematical model, derived from the Navier-Stokes equations of momentum and continuity, which may be accurately used to predict the behavior of conventionally mounted pneumatic sensing systems subject to arbitrary pressure inputs. Numerical techniques for solving the general model are developed. Both step and frequency response lab tests were performed. These data are compared against solutions of the mathematical model. The comparisons show excellent agreement. The procedures used to obtain the lab data are described. In-flight step and frequency response data were obtained. Comparisons with numerical solutions of the mathematical model show good agreement. Procedures used to obtain the flight data are described. Difficulties encountered with obtaining the flight data are discussed.

Nomenclature

A_c	cross-sectional area of pneumatic tubing
c	sonic velocity
C_0	polytropy coefficient
D	pressure tubing cross-sectional diameter
i	spatial index for discretization grid
k	temporal index for discretization grid
L	length of pneumatic tubing
M	maximum number of temporal gridpoints
N	maximum number of spatial gridpoints
$P(x,t)$	pressure function
P_{amb}	ambient pressure
p_{i_k}	i^{th} spatial, k^{th} temporal pressure gridpoint
p_k^{-1}	inverse pressure state, $\frac{1}{p_{N_k}}$
R	acoustic resistance of pneumatic configuration
R_e	Reynolds number of tubing flow
t	time coordinate
$U(x,t)$	velocity function
u_{i_k}	i^{th} spatial, k^{th} temporal velocity gridpoint
V	enclosed transducer volume
x	spatial coordinate
γ	ratio of specific heats for air
δ	discretization parameter, $(\frac{c\Delta t}{\Delta x})^2$
Δt	temporal grid stepsize
Δx	spatial grid stepsize
λ	discretization parameter, $1 + R\Delta t/\rho$
μ	dynamic viscosity of air
ξ	polytropy heat transfer parameter
$\rho(x,t)$	density function

Introduction

Recent advances in aircraft performance and maneuver capability have dramatically complicated the problem of flight control augmentation. Some control system designs now require that aerodynamic parameters such as angle of attack, dynamic pressure, or wing pressure loads be fed back to the control system. The use of aerodynamic parameters as control system feedbacks requires the measurements be recorded with accuracy and high fidelity. Since most aerodynamic parameters must be pneumatically sensed, this is a difficult problem. The primary difficulty in obtaining high-frequency pressure measurements is pressure loss owing to frictional attenuation within the sensing system. Typically, most of the frictional loss comes within the pneumatic tubing used to transmit pressure impulses from the surface of the aircraft to the measurement transducer. To avoid pneumatic attenuation, designers have sought to mount the pressure sensor at the surface of the aircraft (in situ mounting) or, when this is impossible, at least restrict the tubing length to just a few inches. In some cases this is a viable solution. However, when many pressures must be measured in a small surface area, as with a hemispherical airdata sensor, one simply cannot crowd enough pressure transducers into the available space. As a result, the designer must accept whatever compromise is available. Depending upon the aircraft, this means running sizeable lengths of pneumatic tubing from the surface to the pressure transducer.

The emphasis of this paper is on the development of a general numerical technique for accurately predicting

*Aerospace Engineer.

pneumatic attenuation errors when the pressure transducers cannot be mounted in situ. Accurate prediction of pneumatic attenuation errors allow control system designers to provide for adequate feedback-loop robustness. The model is formulated to allow for arbitrary pressures to be input to the sensing system. Numerical techniques for solving the mathematical model are developed. The model is verified by comparing both laboratory and flight data.

Background

As mentioned in the Introduction, for many flight test applications pressure-sensing devices cannot be easily or practically mounted flush to the aircraft skin (in situ mounting). To transmit pressure change at the surface to the transducer, a length of connective tubing is used. Pressure variations at the surface propagate as waves from the upstream end through the connective tubing to the transducer. The wave propagation is damped by frictional attenuation along the walls of the tubing. The wave damping manifests itself as spectral attenuation of the pressure response and produces both a magnitude attenuation and a phase lag. When the wave reaches the downstream end of the tubing, it is reflected back up the tube and may either damp or amplify incoming pressure waves leading to spectral distortion.

A considerable body of information concerning the effects of pneumatic attenuation is available. Early attempts made use of acoustical–electrical analogs to derive time-dependent low-order linear models to approximate pneumatic attenuation.[1,2] Such analyses, although of some predictive value, are not based on rigorous aerodynamic principles and have little generality. Later analyses were based on more rigorous approaches using the equations of momentum and continuity. Such analyses lead to response models for specialized pressure inputs, such as step inputs,[3] ramp inputs,[4] and sinusoidal inputs.[5,6] These analyses, while accurately predicting the pressure response for their prescribed types of inputs, are unable to predict the behavior of pneumatic systems subjected to arbitrary pressure inputs. A more general mathematical model must be developed.

Derivation of Mathematical Model

This section presents the idealized configuration to be analyzed first. Next the Navier-Stokes equations of momentum and continuity are presented. The equations of momentum and continuity are coupled to give a single nonlinear partial differential equation for pressure in terms of position and time. The nonlinear equation is linearized to give a damped wave equation. Finally, the initial and boundary conditions are developed.

Idealized Configuration Geometry

The sensor configuration is modeled as a straight cylindrical tube with an axisymmetric volume attached to its downstream end. The tube represents the transmission line from the surface to the sensor, and the attached volume represents the internal volume of the pressure transducer. The tube is considered to be of constant radius R, with length L. The attached volume V is assumed to be a constant. A longitudinal coordinate x is measured from the upstream end of the tube, and a time coordinate t is measured forward from some initial time t_0. Pressure, density, temperature, and the radial average flow velocity within the tube are considered to be functions of only x and t. These quantities are represented by the symbols $P(x,t)$, $\rho(x,t)$, $T(x,t)$, and $U(x,t)$, respectively. The idealized configuration is depicted in Fig. 1.

Navier-Stokes Equations

The Navier-Stokes equations, contingent on the aforementioned assumptions, are given by Stephens and Bate[7] as

(i) continuity

$$\frac{\partial \rho(x,t)}{\partial t} + \frac{\partial [\rho(x,t)U(x,t)]}{\partial x} = 0 \qquad (1)$$

(ii) momentum

$$\rho \frac{\partial U(x,t)}{\partial t} + \frac{\partial P(x,t)}{\partial x} + RU(x,t) = 0 \qquad (2)$$

The term R in equation (2) is referred to as the acoustic resistance and represents the damping effects of viscosity. For laminar flow the value of R may be shown to be

$$R = \frac{32\mu}{D^2} \qquad (3)$$

where μ is the local dynamic viscosity of air. For turbulent flow conditions, the friction coefficient may be estimated using Blasius' empirical law[8] to give

$$R = 0.1582 R_e^{\frac{3}{4}} \frac{\mu}{D^2} \qquad (4)$$

Empirical data presented in Schlicting[8] indicate that pipe flow transitions from laminar to turbulent for Reynolds numbers above 2300.

Reduction to Nonlinear Wave Equation

If the density behind the pressure wave front at any given time is assumed to be independent of position, and the wave process is assumed to be polytropic[4] where

$$\frac{P}{\rho^{\xi}} = C_0 \qquad (5)$$

equations (1) and (2) may be combined to form a single nonlinear pressure wave equation

$$\frac{\partial^2 P(x,t)}{\partial t^2} + \frac{R}{\rho(t)}\frac{\partial P(x,t)}{\partial t} = \frac{\xi}{\gamma}c^2\frac{\partial^2 P(x,t)}{\partial x^2} + \frac{1}{\xi P(x,t)}\left[\frac{\partial P(x,t)}{\partial t}\right]^2 \tag{6}$$

where γ is the ratio of specific heats, and c is the local sonic velocity. For the current analysis, it is assumed that the flow velocities are low, hence c is approximately constant. The parameter ξ, known as the heat transfer parameter, satisfies $1 \leq \xi \leq \gamma$. If air is the fluid medium, and pressure changes are not large, then $\xi = \gamma = 1.4$ is sufficiently accurate.

Linearization of Nonlinear Wave Equation

Equation (6) may be effectively linearized by noting that

$$P(x,t) = \frac{c^2}{\gamma}\rho(x,t)$$

Substituting into the last term on the right-hand side of equation (6) and regrouping gives

$$\frac{\partial^2 P(x,t)}{\partial t^2} + \left[\frac{R - \frac{\partial P(x,t)}{\partial t}\frac{\gamma}{\xi c^2}}{\rho(t)}\right]\frac{\partial P(x,t)}{\partial t} = \frac{\xi}{\gamma}c^2\frac{\partial^2 P(x,t)}{\partial x^2} \tag{7}$$

Assuming that input pressure rates are not large, an order of magnitude analysis for a typical pressure sensing system[4] indicates

$$R \gg \frac{\partial P(x,t)}{\partial t}\frac{\gamma}{\xi c^2} \tag{8}$$

Thus equation (7) is effectively linearized to give

$$\frac{\partial^2 P(x,t)}{\partial t^2} + \left[\frac{R}{\rho(t)}\right]\frac{\partial P(x,t)}{\partial t} = \frac{\xi}{\gamma}c^2\frac{\partial^2 P(x,t)}{\partial x^2} \tag{9}$$

Equation (9) is simply the classical wave equation with time variable parameters. The pressure variation within the tube can be visualized as the propagation of a longitudinal compression wave.

Development of Initial and Boundary Conditions

To complete the mathematical model, the initial and boundary conditions must still be defined. The initial conditions will be defined by assuming that at time t_0, the system is at rest. As a result the initial pressure and velocity at all stations are prescribed to be

$$P(x,0) = P_0, \quad U(x,0) = 0 \tag{10}$$

The boundary condition at the upstream of the tube is prescribed

$$P(0,t) = P_i(t) \tag{11}$$

The boundary condition at the downstream end of the tube may be obtained by satisfying the equations of continuity and momentum at the downstream end to give

$$\frac{\frac{dP_L(t)}{dt}}{P_L(t)} = \frac{\xi A_c U_L(t)}{V} \tag{12}$$

and,

$$\rho\frac{dU_L(t)}{dt} + RU_L(t) + \left[\frac{\partial P(x,t)}{\partial x}\right]|_L = 0 \tag{13}$$

where A_c is the cross-sectional area of the tube.

Numerical Solution of Pneumatic Attenuation Model With Arbitrary Inputs

The mathematical model given by equations (9), (10), (11), (12), and (13) is to be solved numerically using an implicit-differencing technique. The pressure function is approximated by a series of spatially and temporally discrete gridpoints, with partial derivative operators being approximated by finite differences. For each temporal recursion, the entire spatial grid is solved, and the differential equation for the downstream boundary is updated by numerical integration.

Finite Difference Approximation of Wave Equation

As previously mentioned, the pressure function will be approximated by a series of discrete gridpoints

$$P(x,t) = p_{i_k}$$

and

$$U(x,t) = u_{i_k}$$

with partial derivatives being approximated by difference operators; that is, first derivatives are approximated by

$$\frac{\partial P(x,t)}{\partial t} = \frac{p_{i_{k+1}} - p_{i_k}}{\Delta t} \tag{14}$$

and

$$\frac{\partial P(x,t)}{\partial x} = \frac{p_{i+1_{k+1}} - p_{i_{k+1}}}{\Delta x} \tag{15}$$

The index i represents the i'th spatial gridpoint, and the index k represents the k'th temporal gridpoint; while Δx and Δt represent the spatial and temporal distances between the discrete gridpoints. The difference operators are substituted into equation (9) and rearranged to give the recursive relationship

$$-\lambda p_{i+1_{k+1}} + (\delta+2\lambda)p_{i_{k+1}} - \lambda p_{i-1_{k+1}} = -(1+\delta)p_{i_k} - p_{i_{k-1}} \tag{16}$$

where $\lambda = (c\Delta t/\Delta x)^2$ and $\delta = 1 + [R\Delta t/\rho(t)]$. Equation (16) must be satisfied for

$$i = 1, 2, \ldots M, \quad M = \frac{L}{\Delta x}, \text{and}$$

$$k = 1, 2, \ldots N, \quad N = \frac{t - t_0}{\Delta t}$$

At temporal gridpoint k+1, the spatial grid may be written in matrix form as the symmetric tridiagonal system

$$\begin{bmatrix} \delta+2\lambda & -\lambda & 0 & \cdots & \cdots \\ -\lambda & \delta+2\lambda & -\lambda & \cdots & \cdots \\ 0 & -\lambda & \delta+2\lambda & \cdots & \cdots \\ \cdots & \cdots & \cdots & \cdots & \cdots \\ 0 & 0 & 0 & \cdots & \cdots \\ 0 & 0 & 0 & \cdots & \cdots \\ 0 & 0 & 0 & \cdots & \cdots \end{bmatrix}$$

$$\begin{bmatrix} \cdots & 0 & 0 & 0 \\ \cdots & 0 & 0 & 0 \\ \cdots & 0 & 0 & 0 \\ \cdots & \cdots & \cdots & \cdots \\ \cdots & \delta+2\lambda & -\lambda & 0 \\ \cdots & -\lambda & \delta+2\lambda & -\lambda \\ \cdots & 0 & -\lambda & \delta+2\lambda \end{bmatrix} \begin{bmatrix} p_{1_{k+1}} \\ p_{2_{k+1}} \\ p_{3_{k+1}} \\ \cdots \\ p_{M-3_{k+1}} \\ p_{M-2_{k+1}} \\ p_{M-1_{k+1}} \end{bmatrix} =$$

$$\begin{bmatrix} (1+\delta)p_{1_k} \\ (1+\delta)p_{2_k} \\ (1+\delta)p_{3_k} \\ \cdots \\ (1+\delta)p_{M-3_k} \\ (1+\delta)p_{M-2_k} \\ (1+\delta)p_{M-1_k} \end{bmatrix} - \begin{bmatrix} p_{1_{k-1}} \\ p_{2_{k-1}} \\ p_{3_{k-1}} \\ \cdots \\ p_{M-3_{k-1}} \\ p_{M-2_{k-1}} \\ p_{M-1_{k-1}} \end{bmatrix} + \begin{bmatrix} \lambda p_{0_{k+1}} \\ 0 \\ 0 \\ \cdots \\ 0 \\ 0 \\ \lambda p_{N_{k+1}} \end{bmatrix} \quad (17)$$

Evaluation of Initial and Boundary Conditions

The initial condition and the upstream boundary condition are given explicitly by equations (10) and (11). The downstream boundary condition, given by equations (12) and (13), must be evaluated by integrating with respect to time. Unfortunately, the boundary condition given by equation (12) is unstable for positive values of $U_L(t)$. This instability requires reformulating the downstream boundary condition in terms of an inverse pressure state. This reformulation, which will circumvent instability problems, follows. Solving equation (13) for $U_L(t)$ and substituting into equation (12) gives

$$\frac{\frac{dP_L(t)}{dt}}{P_L(t)} = -\frac{\xi A_c}{VR}\left[\rho\frac{dU_L(t)}{dt} + \frac{\partial P(x,t)}{\partial x}\,|_L\right] \quad (18)$$

Equation (18) may be transformed to a linear equation by defining an inverse pressure state

$$P^{-1}(t) = \frac{1}{P_L(t)}$$

and substituting into equation (18). Regrouping and integrating from temporal indices k to $k+1$ gives

$$p_{k+1}^{-1} = \frac{1}{[\,1 + \frac{\xi A_c \Delta t}{RV^1 \Delta x} p_{N-1_{k+1}}\,]} p_k^{-1} + \frac{\frac{\xi A_c \Delta t}{RV^1 \Delta x}[\,\frac{\gamma \Delta x(\dot{u}_{N_{k+1}} - u_{N_k})}{c^2 \Delta t} + 1\,]}{[\,1 + \frac{\xi A_c \Delta t}{RV^1 \Delta x} p_{N-1_{k+1}}\,]} \quad (19)$$

Equation (19) is a stable reformulation of equation (12) and may be used to evaluate the downstream pressure at each temporal gridpoint.

An implicit algorithm is used for solving equation (9), subject to the constraint of equations (10), (11), (13), and (19). The method requires iteration to convergence at each temporal gridpoint. Each temporal recursion consists of three separate steps: a prediction step, a correction step, and an iteration step. The details, since they are mostly concerned with bookkeeping and stability checking, will not be presented.

Verification of Mathematical Model

At this point, it is appropriate to switch emphasis towards *verification* of the model. Empirical verification of the mathematical model is presented in two steps in this section. First, numerical solutions are compared to laboratory data. Specifically, numerical solutions are compared to data obtained from step response and frequency response laboratory experiments. Second, numerical solutions are compared to actual flight data obtained from a specifically designed experiment. The flight data comparisons aid in establishing the *applicability* of the *mathematical model* to *realistic* pressure measurement configurations.

Laboratory Step Response Tests

Step Response Test Equipment and Procedures. This test assembly was designed to demonstrate the effects of pneumatic attenuation upon step inputs. The general procedure consisted of comparing the response of an in situ mounted reference transducer to the response of a test transducer mounted at the end of a sizable length of pneumatic tubing. A $\frac{1}{2}\ \frac{lbf}{in.^2}$ step was input to the system using an evacuated chamber and an electrically actuated solenoid valve. In order to simulate altitude effects, the experiment was designed to allow the tests to be performed at a variety of ambient pressures.

Results of Step Response Tests. The results from the step response tests are now compared against numerical solutions of the mathematical model. Figures 2 and 3 present sample step response time histories. In these figures, the solid line represents the response of the test transducer as measured in the lab, the short dashed line represents the numerically com-

puted response of the test sensor, and the hashed line represents the step input. Figure 2 depicts the response of a test configuration with 40 ft of 0.081 in. steel tubing at 2300 ft simulated altitude. Figure 3 depicts the response of a test configuration with 20 ft of 0.081 in. steel tubing at 20,000 ft simulated altitude. The agreements are excellent.

Laboratory Frequency Response Tests

Frequency Response Test Equipment and Procedures. This test assembly was designed to demonstrate the effects of pneumatic attenuation upon sinusoidal inputs. The general procedure consisted of comparing the relative frequency responses of an in situ mounted transducer to a transducer mounted at the end of a test section of pneumatic tubing. A piston-actuated, electromechanical acoustical amplifier was used to input sinusoidal waves of prescribed frequencies and amplitudes to the measurement configuration. The base pressure within the amplifier cylinder cavity could be raised or lowered to simulate a desired altitude. Tests were repeated for each of the tubing test sections at a variety of base pressures.

Results of the Lab Frequency Response Tests. Selected results of the frequency response tests are now compared against numerical solutions of the mathematical model. Figures 4 and 5 present sample Bode plots resulting from the lab tests. Both magnitude and phase angle plots are presented. In these figures, the solid line represents the frequency response of the test transducer as measured in the lab, and the short dashed line represents the numerically computed frequency response. Figure 4 depicts the frequency response of a test configuration with 24.5 in. of 0.046 in. steel tubing at 2300 ft simulated altitude. Figure 5 depicts the frequency response of a test configuration with 24.5 in. of 0.046 in. steel tubing at 20,000 ft simulated altitude. As with the step response data, the matches are excellent.

The comparisons of this section indicate that the ability of the model to predict the response of simple pressure measurement configurations is quite good. The model is equally accurate for step and frequency response predictions.

Comparisons of Flight Data to Numerical Solutions of Mathematical Model

With the accuracy of the mathematical model in predicting the behavior of simple configurations under a controlled laboratory environment being demonstrated, it now becomes pertinent to demonstrate the applicability of the model to an actual flight test sensing system. Flight tests which approximated both step and frequency response experiments were performed.

Flight Test Equipment and Procedures. The following section describes the configuration that was used to obtain the flight test data. Basically, the configuration consisted of a matrix of five pressure sensors with ports clustered at the 10 percent chord and 20 percent span on the upper surface of the right-hand wing of an F-15 aircraft. The flight test configuration, located on the right-hand wing, is shown in Fig. 6.

Two of the ports were configured to serve as reference sensors. The other three ports were configured to serve as test sensors. The reference transducers were mounted so as to produce little pneumatic attenuation in the pressure measurements. The test sensors were mounted at the end of tubing sections similar to those used in the lab tests. The tubing sections were interchangeable to allow for the testing of various tubing sections.

Using the following technique, step response data were obtained at a variety of altitudes from 10,000 to 40,000 ft. First, the aircraft was flown at a high subsonic speed until a shock formed downstream of the test matrix. At this point the pilot would perform a windup turn (to the left), thereby increasing the local velocity on the surface of the right-hand wing. This caused the shock wave to move forward until eventually it passed over the sensor matrix. The effect was to introduce a sharp step-like increase in the local pressure. As the pilot rolled out of the turn, the local velocity on the right-hand wing dropped and the shock retreated. The effect was to introduce a sharp step-like drop in the local pressure.

Although pure frequency response data were impossible to obtain in-flight, the following technique proved useful in obtaining a broadband fairly white input to the test matrix. At moderate subsonic speeds, the pilot would roll into a windup turn to the right. At this point the pilot pulled the aircraft into a high angle of attack. The combination of lateral g's and high angle of attack caused mild leading-edge separation. Noisy vortices, which would subsequently impinge upon the sensor matrix, were shed. The spectral content of these vortices was broadband and (beyond 20 Hz) nearly white. Because the vortices were random, no phase coherence could be established between the reference and test sensors.

Results of the Flight Tests. Selected results of the flight tests are now compared against numerical solutions of the mathematical model. Step response data are presented first. The frequency response data will then follow.

Sample step response time histories are presented in Figs. 7 and 8. In these figures the solid line represents the measured response of the reference sensor, the short dashed line represents the numerically computed response of the test sensor, and the hashed line represents the measured response of the test sensor. Depicted are the responses of 2-ft sections of 0.02 and

0.04 in. diameter steel pnuematic tubing at an altitude of 39,800 ft. Again, the agreements are outstanding.

Selected results of the frequency response tests are now compared against numerical solutions of the mathematical model. Figures 9 and 10 present sample Bode plots in which the relative magnitudes of the test and reference sensor measurements are compared against the numerically computed frequency response of the test sensors. In these figures the solid line represents the frequency response of the test transducer (relative to the reference transducer) as measured in-flight, and the hashed line represents the numerically computed frequency response of the test sensor. Figure 9 shows the frequency response of a test configuration with 24.5 in. of 0.04 in. steel tubing at 40,000 ft altitude. Figure 10 depicts the frequency response of a test configuration with 24.5 in. of 0.02 in. steel tubing at 40,000 ft altitude. The comparisons are good.

Conclusions

The mathematical model, derived from the Navier-Stokes equations expressed in one spatial dimension, is essentially a damped wave model. Due to the assumptions required in linearizing the model, it is valid for predicting the behavior of pneumatic measurement configurations in which the rate of change of the pressure within the configuration is not large. Since this is the case for most pneumatic measurement systems, the model has general applicability.

Comparisons of the mathematical model to both lab and flight step and frequency response data indicate that its predictive ability is excellent. The model is capable of predicting the response of a simple measurement configuration for any sort of input. It is thus directly applicable to flight data.

By applying the boundary conditions in the reverse direction (letting the downstream pressure be directly measured and solving continuity and momentum at the upstream end), it is possible to invert the mathematical model to give a compensation routine that may be used to adjust for the effects of pneumatic attenuation. The compensation technique still has some problems with numerical stability and is being further developed at this time.

There are many difficulties with obtaining in situ pressure measurements under a flight environment. Primary difficulties lie with controlling the environment of the sensor, ensuring survivability, and damping out structural noise on the sensor. At this time no adequate technology exists which allows one to practically and cheaply obtain high-quality pressure measurements using in situ mounted sensors. Conventionally mounted sensors with short lengths of pneumatic tubing have been shown herein to give excellent results and are not subject to many of the difficulties encountered with in situ mounted sensors. Using the developed code, the effects of pneumatic attenuation can be identified. Having identified the effects of pneumatic attenuation, the control designer can provide for sufficient robustness in loops that use the pneumatically derived data as feedbacks.

References

[1] Huston, W.B.: *Accuracy of Airspeed Measurements and Flight Calibration Procedures.* NACA Report 919, 1948.

[2] Hougen, J.O.; Martin, O.R.; and Walsh, R.A.: *Dynamics of Pneumatic Transmission Lines.* Control Engineering, vol. 10, no. 9, 1963, pp. 114–117.

[3] Schuder, C.B.; and Binder, R.C.: *The Response of Pneumatic Transmission Lines to Step Inputs.* Journal of Basic Engineering, ASME Transactions, Dec. 1959.

[4] Lamb, J.P.: *The Influence of Geometry Parameters Upon Lag Error in Airborne Pressure Measurement Systems.* WADC TR 57-351, Wright-Patterson AFB, Ohio, July 1957.

[5] Iberall, A.S.: *Attenuation of Oscillatory Pressures in Instrument Lines.* Journal of Research of the National Bureau of Standards, vol. 45, RP2115, July 1950, pp. 85–108.

[6] Berg, H.; and Tijdeman, H.: *Theroetical and Experimental Results for the Dynamic Response of Pressure Measuring Systems.* NLR report F.238, 1965.

[7] Stephens, R.W.B.; and Bate, A.E.: *Acoustics and Vibrational Physics.* St. Martin's Press, New York, 1966.

[8] Schlichting, Hermann: *Boundary Layer Theory.* McGraw-Hill Book Co., New York, 1960.

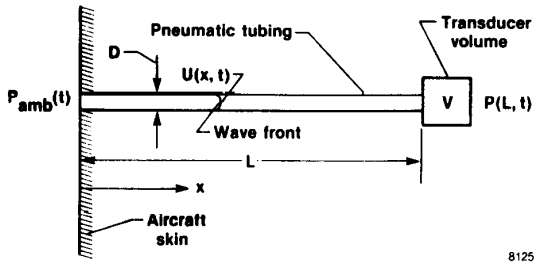

Fig. 1 Schematic of pressure sensing device.

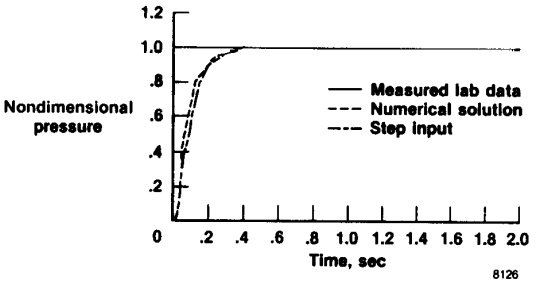

Fig. 2 Step response data: comparisons of lab to mathematical model for L = 40 ft, D = 0.081 in., and altitude = 2300 ft.

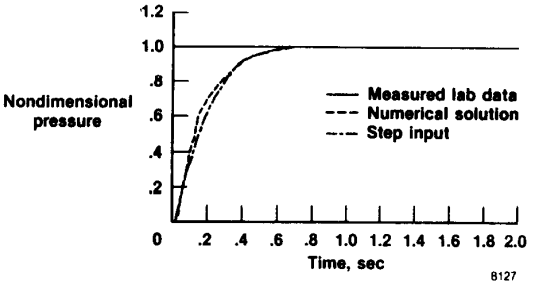

Fig. 3 Step response data: comparisons of lab to mathematical model for L = 40 ft, D = 0.081 in., and altitude = 20,000 ft.

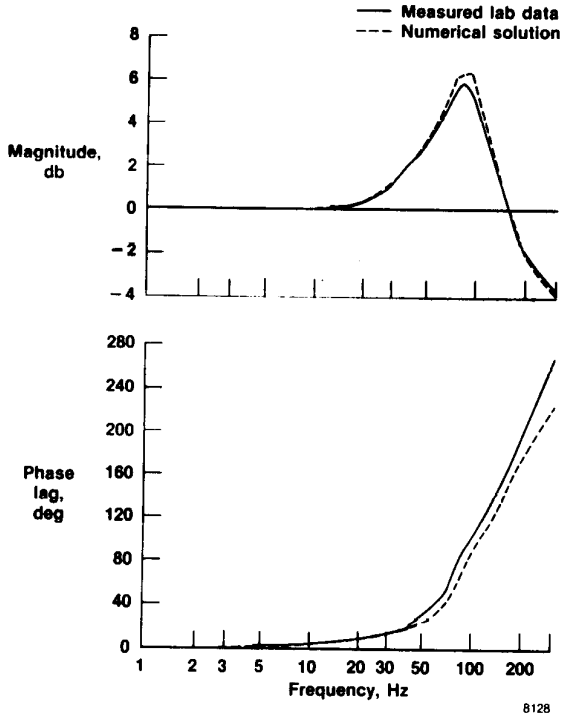

Fig. 4 Frequency response data: comparisons of lab to mathematical model for $L = 24.5$ in., $D = 0.046$ in., and altitude = 2300 ft.

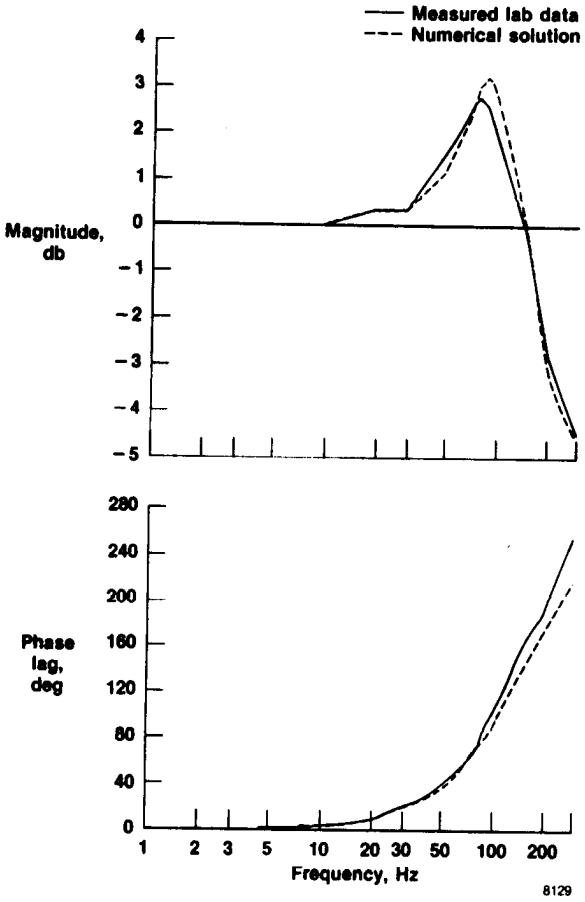

Fig. 5 Frequency response data: comparisons of lab to mathematical model for $L = 24.5$ in., $D = 0.046$ in., and altitude = 20,000 ft.

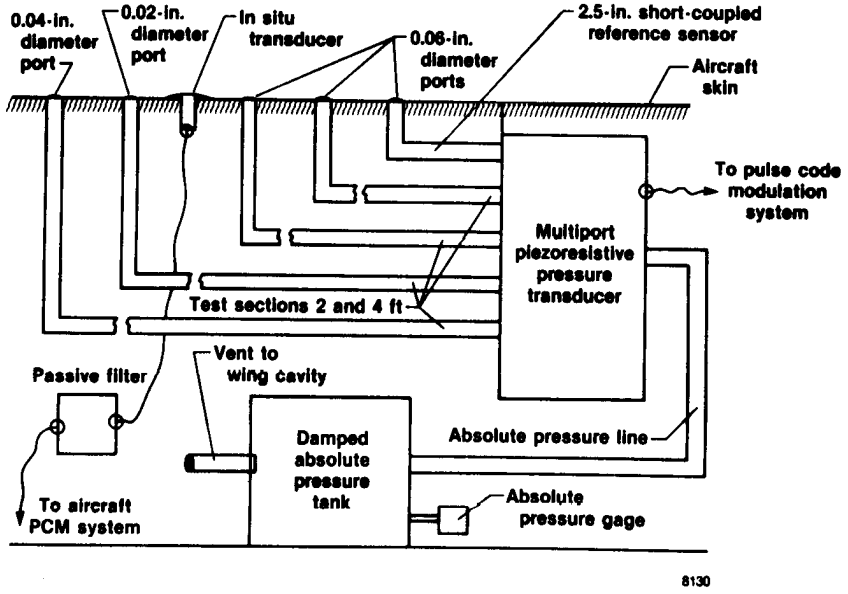

Fig. 6 Experimental configuration used for flight tests.

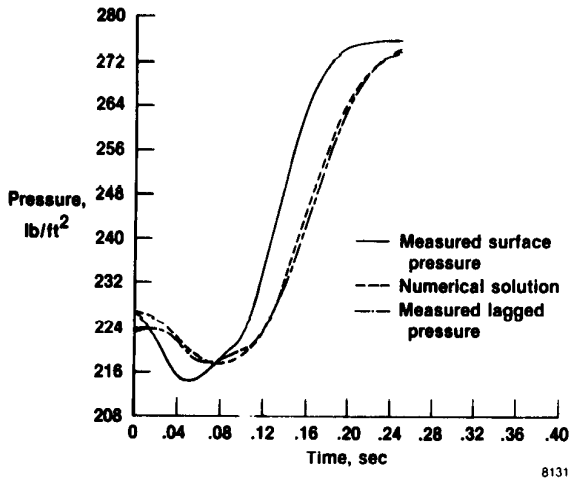

Fig. 7 Step response data: comparisons of flight results to mathematical model for L = 2 ft, D = 0.020 in., and altitude = 39,800 ft.

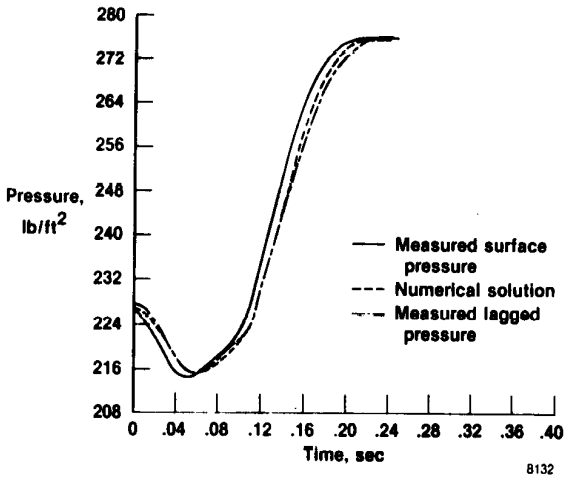

Fig. 8 Step response data: comparisons of flight results to mathematical model for L = 2 ft, D = 0.040 in., and altitude = 39,800 ft.

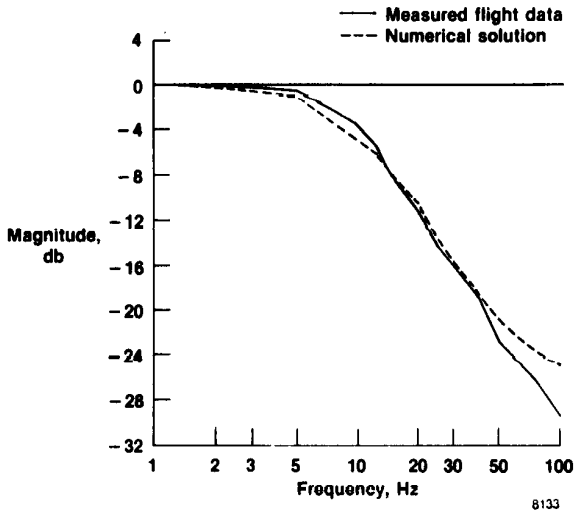

Fig. 9 Frequency response data: comparisons of flight data to mathematical model for L = 24.5 in., D = 0.04 in., and altitude = 40,000 ft.

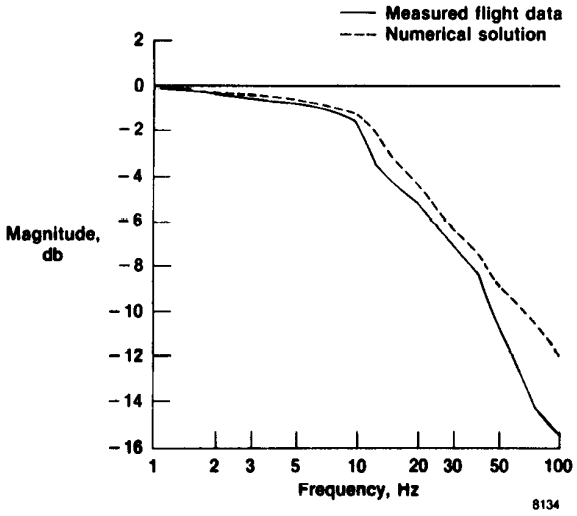

Fig. 10 Frequency response data: comparisons of flight data to mathematical model for L = 24.5 in., D = 0.02 in., and altitude = 40,000 ft.

NASA
National Aeronautics and Space Administration

Report Documentation Page

1. Report No.	2. Government Accession No.	3. Recipient's Catalog No.
NASA TM-100430		

4. Title and Subtitle

Formulation of a General Technique for Predicting Pneumatic Attenuation Errors in Airborne Pressure Sensing Devices

5. Report Date

May 1988

6. Performing Organization Code

7. Author(s)

Stephen A. Whitmore

8. Performing Organization Report No.

H-1462

10. Work Unit No.

RTOP 505-68-31

9. Performing Organization Name and Address

NASA Ames Research Center
Dryden Flight Research Facility
P.O. Box 273, Edwards, CA 93523-5000

11. Contract or Grant No.

13. Type of Report and Period Covered

Technical Memorandum

12. Sponsoring Agency Name and Address

National Aeronautics and Space Administration
Washington, DC 20546

14. Sponsoring Agency Code

15. Supplementary Notes

Prepared for presentation at the AIAA 4th Flight Test Conference, May 18–20, 1988, at San Diego, California.

16. Abstract

Presented is a mathematical model, derived from the Navier-Stokes equations of momentum and continuity, which may be accurately used to predict the behavior of conventionally mounted pneumatic sensing systems subject to arbitrary pressure inputs. Numerical techniques for solving the general model are developed. Both step and frequency response lab tests were performed. These data are compared against solutions of the mathematical model. The comparisons show excellent agreement. The procedures used to obtain the lab data are described. In-flight step and frequency response data were obtained. Comparisons with numerical solutions of the mathematical model show good agreement. Procedures used to obtain the flight data are described. Difficulties encountered with obtaining the flight data are discussed.

17. Key Words (Suggested by Author(s))	18. Distribution Statement
Pneumatic attenuation Pneumatic lag Pressure sensors	Unclassified — Unlimited Subject category 05

19. Security Classif. (of this report)	20. Security Classif. (of this page)	21. No. of pages	22. Price
Unclassified	Unclassified	12	A02

NASA FORM 1626 OCT 86

*For sale by the National Technical Information Service, Springfield, VA 22161-2171.